Accepted Manuscript

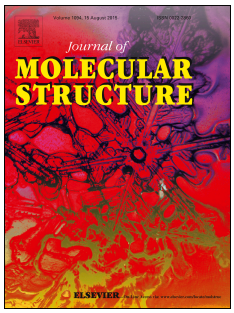

Rh{(η^4-cod) or $(PPh_3)_2$}-Schiff base complexes with a Z′ = 2 structure: Syntheses, spectroscopy, thermalanalyses and DFT/TDDFT

Mohammed Enamullah, Mohammad Ariful Islam, Christoph Janiak

PII: S0022-2860(16)30562-2

DOI: 10.1016/j.molstruc.2016.05.093

Reference: MOLSTR 22607

To appear in: *Journal of Molecular Structure*

Received Date: 4 March 2016

Revised Date: 22 April 2016

Accepted Date: 27 May 2016

Please cite this article as: M. Enamullah, M.A. Islam, C. Janiak, Rh{(η^4-cod) or $(PPh_3)_2$}-Schiff base complexes with a Z′ = 2 structure: Syntheses, spectroscopy, thermalanalyses and DFT/TDDFT, *Journal of Molecular Structure* (2016), doi: 10.1016/j.molstruc.2016.05.093.

Graphical Abstract

Rh{(η^4-cod) or (PPh_3)$_2$}-Schiff base complexes with a Z' = 2 structure: syntheses, spectroscopy, thermalanalyses and DFT/TDDFT

Mohammed Enamullah[a,*], Mohammad Ariful Islam, Christoph Janiak[b]

[a] *Department of Chemistry, Jahangirnagar University, Dhaka-1342, Bangladesh. Email: enamullah@juniv.edu*

[b] *Institute for Inorganic and Structure Chemistry, Heinrich-Heine-University, University Str. 1, D-40225 Düsseldorf, Germany. Email: janiak@uni-duesseldorf.de*

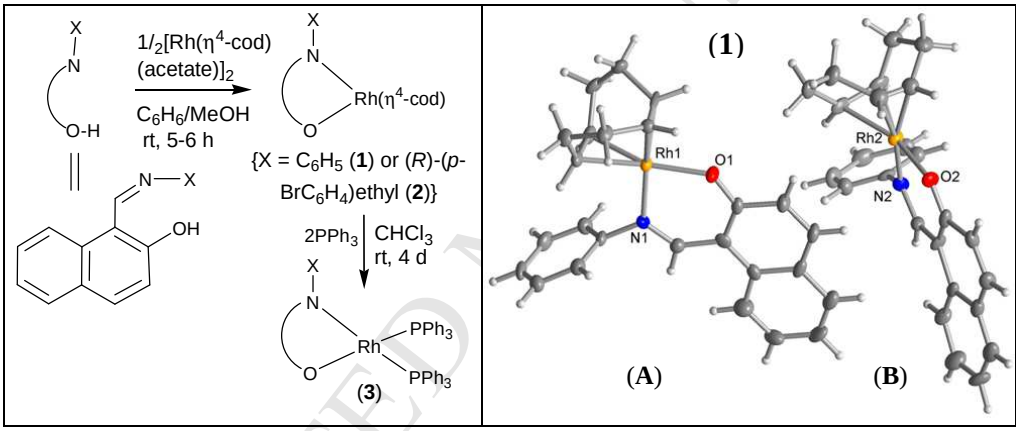

Rh{(η^4-cod) or (PPh_3)$_2$}-Schiff base complexes with a Z' = 2 structure: syntheses, spectroscopy, thermalanalyses and DFT/TDDFT

Mohammed Enamullah[a,*], Mohammad Ariful Islam, Christoph Janiak [b]

[a] *Department of Chemistry, Jahangirnagar University, Dhaka-1342, Bangladesh. Email: enamullah@juniv.edu*

[b] *Institute for Inorganic and Structure Chemistry, Heinrich-Heine-University, University Str. 1, D-40225 Düsseldorf, Germany. Email: janiak@uni-duesseldorf.de*

Abstract

Reaction of Schiff bases with [Rh(η^4-cod)(acetate)]$_2$ (cod = 1,5-cyclooctadiene) provides [Rh(η^4-cod){N-(C_6H_5)-2-oxo-1-naphthaldiminato-κ^2*N,O*}] (**1**) and [Rh(η^4-cod){(*R*)-N-(*p*-BrC_6H_4)ethyl-2-oxo-1-naphthaldiminato-κ^2*N,O*}] (**2**), respectively. Compound **2** reacts with triphenylphosphine (PPh_3) to give [Rh(PPh_3)$_2${(*R*)-N-(*p*-BrC_6H_4)ethyl-2-oxo-1-naphthaldiminato-κ^2*N,O*}] (**3**). Molecular structure determination for **1** reveals that 2-oxo-1-naphthaldiminate ligand is coordinated to the Rh(η^4-cod)-fragment with six-membered *N^O*-chelation in distorted square planar geometry. The structure shows two symmetry-independent molecules in the asymmetric unit to give a Z' = 2 structure. Optimized structures correspond well to the experimental results. Electronic spectra by TDDFT show a combined metal-metal and metal-ligand transitions band at 411 (**1**) or 402 (**2**) nm with the highest MOs contributions of *ca.* 81% for HOMO-1 to LUMO, comparable to the experimental bands. Electronic spectra in different solvents show a negative solvatochromic trend with increasing dielectric constants and acceptor number of solvents, respectively. ^{1}H NMR spectra show two multiplets for exo- and endo-methylene protons, and two boublets for olefin protons of cod-ligand, respectively. ^{31}P NMR spectra show two sets of doublets at δ 38.59 and 39.55 ppm due to two assymetric P-atoms coordinated to the rhodium *trans* to *N* and *O* atoms, respectively in **3**. DSC analyses demonstrate an irriversible phase transformation from crystalline to isotropic liquid phase.

Keywords: Rh(η^4-cod)-fragment; Chiral/achiral Schiff base, Triphenylphosphine; X-ray structure; DFT/TDDFT calculations

1. Introduction

Rh(η^4-cod)-achiral/chiral Schiff base complexes, derived from the reaction between Schiff bases and dinuclear [Rh(η^4-cod)(acetate)]$_2$ (cod = 1,5-cyclooctadiene) are of continued interests because of their uses for asymmetric reduction of ketone and ketone derivatives with substantial (%) ee values [1-4]. In recent years, we have given attentions to synthesize the Rh(η^4-cod)-complexes starting from chiral amino acids/amino alcohols and [Rh(η^4-cod)(acetate)]$_2$ [5-10]. In this connection, we have reported the syntheses, spectroscopy and crystal structures of mononuclear [Rh(η^4-cod)(XY)] (XY = chiral amino carboxxylato) and [Rh(η^4-cod)(AA)](acetate) (AA = chiral amino alchohol) [5-9]. Crystal structures reveal a five-membered *N,O*-chelation of the amino-carboxylate or amino-alcohol to the Rh(η^4-cod)-fragment with distorted tetrahedral geometry. In addition, the di/tri-phosphine ligands (diphos/triphos) readily react with these complexes to yield the cationic [Rh(diphos)$_2$](XY) or neutral [Rh(diphos/triphos)(XY)] complexes [10].

We have further reported the syntheses and spectroscopic characterization of Rh(η^4-cod)-chiral Schiff base complexes including [Rh(η^4-cod)(*R*/*S*-SB)] {SB = N-(Ar)ethyl-salicylaldiminato/naphthaldiminato} [8,11-12], [Rh(η^4-cod)(*R*-HL)](acetate) {HL = 2-(X-benzaldimine)-2-phenylethanol} [13], and [Rh(η^4-cod)(*R*/*S*-HL1 or (*rac*)HL2)] {HL1 = N-2-(salicylaldiminate)-2-phenylethanol, HL2 = N-2-(salicylaldiminate)-1-phenylethanol} [14]. Molecular structure diterminations demonstrates that a six-membered *N,O*-chelation of the deprotonated Schiff base ligands to the Rh(η^4-cod)-fragment with distorted square planar geometry.

The present paper, in continuation, reports the results of syntheses, spectroscopy and thermal analyses on [Rh(η^4-cod){N-(C_6H_5)-2-oxo-1-naphthaldiminato-κ^2*N,O*}] (**1**), [Rh(η^4-cod){(*R*)-N-(*p*-BrC_6H_4)ethyl-2-oxo-1-naphthaldiminato-κ^2*N,O*}] (**2**), and [Rh(PPh_3)$_2${(*R*)-N-(*p*-BrC_6H_4)ethyl-2-oxo-1-naphthaldiminato-κ^2*N,O*}] (**3**), respectively. Single crystal structure for **1** has been dertermined. The optimized geometry and electronic spectra are studied by DFT/TDDFT, which are compared with the experimental results.

2. Experimental

Materials and physical measurements

All reactions were carried out under an atmosphere of dry nitrogen using standard Schlenk tube techniques. Solvents used were dried and deoxygenated under nitrogen prior to use. FT-

IR (KBr disc) and ATR spectra were recorded on a Thermo Scientific spectrometer (Nicolet iS10) at ambient temperature. UV-Vis. spectra were obtained with a Shimadzu UV 3150 spectrophotometer in different solvents at 20 ^{o}C. Elemental analyses were done on a Vario EL instrument from Elementar Analysensysteme, GmbH. Differential scanning calorimeter (DSC) analyses were performed on a Shimadzu DSC-60 at the range of 30-260 ^{o}C (before decomposition temperature) with a rate of 10 K min^{-1}. ^{1}H NMR spectra were run on Bruker Avance DPX 400 spectrometer operating at 400 MHz (^{1}H), respectively at 20 ^{o}C. EI/ESI-MS: Thermo-Finnigan TSQ 700 .$^{79/81}$Br isotopic distribution patterns are clearly visible following the peaks at *m*/*z* 602, 586, 376 and 183 in **2**, and at 994, 756/716, 557, 367 in **3**. The starting dinuclear [Rh(η^4-cod)(acetate)]$_2$ was synthesized from [Rh(η^4-cod)Cl]$_2$ according to our previous literature [5-8]. Syntheses of the Schiff base ligands, N-(C_6H_5)-2-hydroxy-1-naphthaldimine (HSB1) and (*R*)-N-(*p*-BrC_6H_4)ethyl-2-hydroxy-1-naphthaldimine (HSB2) were described in our previous literature [7,11-12].

*2.1. Synthesis of compounds **1** and **2***

Two equivalents of N-(C_6H_5)-2-oxo-1-naphthaldimine (HSB1) (0.40 mmol) and one equivalent of [Rh(η^4-cod)(acetate)]$_2$ (0.20 mmol) were dissolved in 10 mL of C_6H_6/MeOH (5:1, v/v). The solution was stirred for about 6 h at room temperature, and color changed from red-orange to bright-yellow. The solvent of reaction mixture was evaporated in *vacuo* and obtained the yellow product. The product was then dissolved again in 10 mL of C_6H_6/MeOH (5:1, v/v) and stirred the solution for another 30 min. Evaporated the solvent again in *vacuo* and this procedure was repeated two times. The product was finally dried in *vacuo* (0.1-0.2 mbar) at 40 ^{o}C and obtained bright yellow compound **1**. The same procedure was followed for synthesis of compound **2**.

*2.1.1. [Rh(η^4-cod){N-(C_6H_5)-2-oxo-1-naphthaldiminato-κ^2N,O}], [Rh(η^4-cod)(SB1)] (**1**):*

Yield: 130 mg (71%); $C_{25}H_{24}NORh$ (457.38): calcd. C 65.65, H 5.29, N 3.06 %, found: C 65.64, H 5.93, N 2.46 %; FT-IR (KBr): ν = 3042, 3007, 2958, 2922 w (C-H), 1615, 1602 vs (C=N), and 1575, 1534 vs (C=C) cm^{-1}; EI-MS (70 eV): *m*/*z* (%) = 457 (100) ([M]$^{+}$), 349 (15) ([Rh(SB1)]$^{+}$), 321 (20) ([Rh(SB1)-CO]$^{+}$), 246 (10) ([HSB1-H]$^{+}$), and 218 (35) ([HSB1-CHO]$^{+}$); ^{1}H NMR (200 MHz, $CDCl_3$): δ = 1.77 (m, 4H, C*H*$_2$cod$_{exo}$), 2.42 (m, 4H, C*H*$_2$cod$_{endo}$), 3.30 (d, *J* = 2.4 Hz, 1H, C*H*cod), 4.61 (d, *J* = 2.4 Hz, 2H, C*H*cod), 7.10 (d, *J* = 7.8 Hz, 2H, *H*-Ar), 7.24 (dt, *J* = 7.8, 1.8, 2H, *H*-Ar), 7.36 (m, 3H, *H*-Ar), 7.55 (m, 2H, *H*-

Ar), 7.68 (m, 2H, *H*-Ar), and 8.88 (d, *J* = 2.0 Hz, 1H, C*H*N) ppm. ^{1}H NMR (200 MHz, DMSO-d_6): δ = 1.84 (m, 4H, CH_2cod$_{exo}$), 2.37 (m, 4H, CH_2cod$_{endo}$), 3.40 (d, *J* = 4.6 Hz, 2H, C*H*cod), 4.20 (d, *J* = 5.6 Hz, 2H, C*H*cod), 7.02 (d, *J* = 9.0 Hz, 1H, *H*-Ar), 7.22 (d, *J* = 7.7 Hz, 1H, *H*-Ar), 7.33 (t, *J* = 6.4, 1H, *H*-Ar), 7.45 (m, 3H, *H*-Ar), 7.77 (m, 3H, *H*-Ar), 7.91 (d, *J* = 9.3 Hz, 1H, *H*-Ar), 8.04 (d, *J* = 8.8 Hz, 1H, *H*-Ar), and 8.94 (s, 1H, C*H*N) ppm.

*2.1.2. [Rh(η^4-cod){(R)-N-(p-BrC_6H_4)ethyl-2-oxo-1-naphthaldiminato-κ^2N,O}], [Rh(η^4-cod)(SB2)] (**2**)*

Yield: 155 mg (69%); $C_{27}H_{27}$BrNORh (564.33): calcd. C 57.47, H 4.82, N 2.48 %, found: C 57.21, H 5.07, N 2.55 %; IR (KBr): ν = 3055, 3010, 2950 w (νH-C), 1611vs, 1602vs (νC=N), and 1584, 1533vs (νC=C) cm^{-1}; ESI(+)-MS (in methanol): *m/z* (%) = 602 (4) ([M+K]$^+$), 586 (8) ([M+Na]$^+$), 376 (6) ([HSB2+Na]$^+$), 262 (100) ([{C_6H_5(CH_3)CNH}$_2$+Na]$^+$), and 183 (38) ([$CH_3CHC_6H_4$Br]$^+$) ($^{79/81}$Br isotopic distribution is clearly visible following the peaks at 602, 586, 376, 183, respectively). ^{1}H NMR (400 MHz, $CDCl_3$): δ = 1.74 (d, *J* = 6.8 Hz, 3H, CH_3), 2.01 (m, 4H, CH_2cod$_{exo}$), 2.56 (m, 4H, CH_2cod$_{endo}$), 3.87 (d, *J* = 7.0 Hz, 2H, C*H*cod), 4.46 (q, *J* = 6.6Hz, 1H, C*H*), 4.67 (d, *J* = 7.5 Hz, 2H, C*H*cod), 7.04 (d, *J* = 9.1 Hz, 1H, *H*-Ar), 7.17 (t, *J* = 7.4 Hz, 1H, *H*-Ar), 7.31 (m, 3H, *H*-Ar), 7.46 (d, *J* = 8.4 Hz, 1H, *H*-Ar), 7.55 (d, *J* = 7.8 Hz, 2H, *H*-Ar), 7.60 (d, *J* = 7.8 Hz, 1H, *H*-Ar), 7.68 (d, *J* = 9.2 Hz, 1H, *H*-Ar), and 8.87 (s, 1H, C*H*N) ppm.

*2.2. Synthesis of compound **3***

A mixture of compound **2** with little excess of PPh_3 in $CHCl_3$ was stirred for 3-4 d at room temperature under nitrogen atmosphere. Color changed from bright orange to red-orange. The progress of reaction was monitored by taking ^{31}P NMR spectra after 4h, 24h, and finally, after 4d. The results indicate the formation of [Rh(η^4-cod)(PPh_3)$_2$]$^+$, [Rh(PPh_3)$_4$]$^+$ and PPh_3(O) species in addition to the expected product during the reaction process, evidenced by ^{31}P NMR signals. The product was filtered off, washed with diethylether, and dried in *vacuo* at 40 ^{o}C, for several hours and obtained the red-orange product of **3**. The compound is very sensitive to air and immediately formed the oxidative adducts.

*2.2.1. [Rh(PPh_3)$_2${(R)-N-(p-BrC_6H_4)ethyl-2-oxo-1-naphthaldiminato-κ^2N,O}], [Rh(PPh_3)$_2$(SB2)] (**3**)*

Yield: 235 mg (60%); IR (KBr): ν = 3060, 3030, 3006, 2940 w (νH-C), 1614vs, 1606vs (νC=N), and 1588, 1537vs (νC=C) cm^{-1}. ESI (+)-MS (in acetonitrile): *m/z* (%) 716 (22) ($[M-PPh_3]^+$), 557 (30) ($[(PPh_3O)_2+H]^+$), 495 (8) ($[Rh(SB2)+K]^+$), 367 (70) ($[\{CH(CH_3)(C_6H_4Br)\}_2+H]^+$), and 279 (100) ($[(PPh_3O)+H]^+$). ESI (+)-MS (in ethanol): *m/z* (%) 994 (1.0) ($[M(O)]^+$), 857 (60) ($[(PPh_3O)_3+K]^+$), 756 (18) ($[M-PPh_3+K]^+$), 579 (100) ($[(PPh_3O)_2+Na]^+$), 557 (95) ($[(PPh_3O)_2+H]^+$), 478 (20) ($[Rh(SB2)+Na]^+$), 367 (80) ($[\{(C_6H_4Br)CH(CH_3)\}_2+H]^+$), and 279 (85) ($[(PPh_3O)+H]^+$) ($^{79/81}$Br isotopic distribution patterns are clearly visible following the peaks at 994, 756 or 716, 367, respectively). ^{1}H NMR (300 MHz, $CDCl_3$): δ = 1.85 (m, 3H, C*H*$_3$), 4.35 (m, 1H, C*H*), 7.08 (m, 30H, *H*-PPh_3), 7.12 (m, 2H, *H*-Ar), 7.40 (m, 4H, *H*-Ar), 7.50 (m, 1H, *H*-Ar), 7.69 (m, 3H, *H*-Ar), and 8.45 (m, 1H, C*H*N) ppm.

2.3. X-ray crystallography

Data Collection: Bruker APEX-II with CCD area-detector, temperature 172(2) K, Mo-Kα radiation (λ = 0.71073 Å), graphite monochromator, ω-scans, data collection and cell refinement with SMART [15] data reduction with SAINT [15], experimental absorption correction with SADABS [16]. *Structure Analysis and Refinement*: The structure was solved by direct methods (SHELXS-97) [17']; refinement was done by full-matrix least squares on F^2 using the SHELXL-97 program suite [17]. All non-hydrogen positions were found and refined with anisotropic temperature factors. Hydrogen atoms on C (CH, CH, and CH_2) were calculated with appropriate riding models (AFIX 3, 13, and 23, respectively) and Ueq(H) = 1.2 Ueq(C). Details of X-ray structure determination and data refinement are provided in Table 1. Graphics were drawn with DIAMOND (Version 3.0e) [18].

Table 1. Crystal data and structure refinement for **1**.

Empirical formula	C25H24NORh
M (g mol^{-1})	457.36
Crystal size (mm)	0.28 x 0.19 x 0.13
Temperature (K)	172(2)
θ range (°)	0.97 to 25.00
h; *k*; *l* range	–15, 27; –11, 9; ±23
Crystal system	Monoclinic
Space group	P21/c
a, *b*, c (Å)	23.1368(17), 9.3168(7), 20.1129(15)
β (deg.)	115.3990(10)
V ($Å^3$)	3916.5(5)
Z/*D* (calc/g cm^{-3})	8/1.551
F(000)/μ (mm^{-1})	1872/0.887

Max/min transmission	0.8934/0.7892
Reflections collected	19242
Independent reflections (R_{int})	6878 (0.0375)
Data / restraints / parameters	6878/0/490
Largest diff. peak and hole ($\Delta\rho$ /e Å^{-3})	4.061/–1.406
R_1/wR_2 [$I > 2\sigma(I)$] [a]	0.0763/0.1833
R_1/wR_2 (all reflect.) [a]	0.0827/0.1866
Goodness-of-fit on F^2 [b]	1.245
Absolute structure parameter [19]	–0.04(2)

– [a] $R_1 = [\Sigma(\|F_o\| - |F_c|\|) / \Sigma |F_o|]$; $wR_2 = [\Sigma [w(F_o^2 - F_c^2)^2]/\Sigma[w(F_o^2)^2]]^{1/2}$. – [b] Goodness-of-fit = $[\Sigma [w(F_o^2 - F_c^2)^2] /(n-p)]^{1/2}$.

2.4. Computational method

For computation, the initial geometries were generated from the X-ray structures of **1** and **2** [12], respectively. All calculations were performed with the Gaussian 09 software package [20]. The gas phase equilibrium geometries of both compounds were optimized and then the vibrational frequencies were calculated with density functional theory (DFT) using B3LYP functional with SDD basis sets. The absence of any imaginary frequencies confirmed that the stationary points correspond to minima on the Potential Energy Surface. To rationalize the experimental electronic spectra, the excited state properties were studied by time-dependent density functional theory (TDDFT) with B3LYP/SDD, incorporating PCM (Polarization Continuum Model) using chloroform as a solvent [9,21]. In TDDFT calculations, 72 excitation states were considered (Table S1-S2). After computation, the molecular orbital (MOs) calculations were conducted using same level of theory.

3. Results and discussion

3.1. Syntheses of the compounds

Reaction of Schiff base ligand N-(C_6H_5)-2-hydroxy-1-naphthaldimine or (*R*)-N-(*p*-BrC_6H_4)ethyl-2-hydroxy-1-naphthaldimine with dinuclear [Rh(η^4-cod)(acetate)]$_2$ gives the mononuclear [Rh(η^4-cod){N-(C_6H_5)-2-oxo-1-naphthaldiminate}] (**1**) or [Rh(η^4-cod){(*R*)-N-(*p*-BrC_6H_4)ethyl-2-oxo-1-naphthaldiminate}] (**2**) in C_6H_6/MeOH (5:1, v/v) (Scheme 1). The triphenylphosphine (PPh_3) reacts with **2** to provide the [Rh(PPh_3)$_2${(*R*)-N-(*p*-BrC_6H_4)ethyl-2-oxo-1-naphthaldiminate}] (**3**).

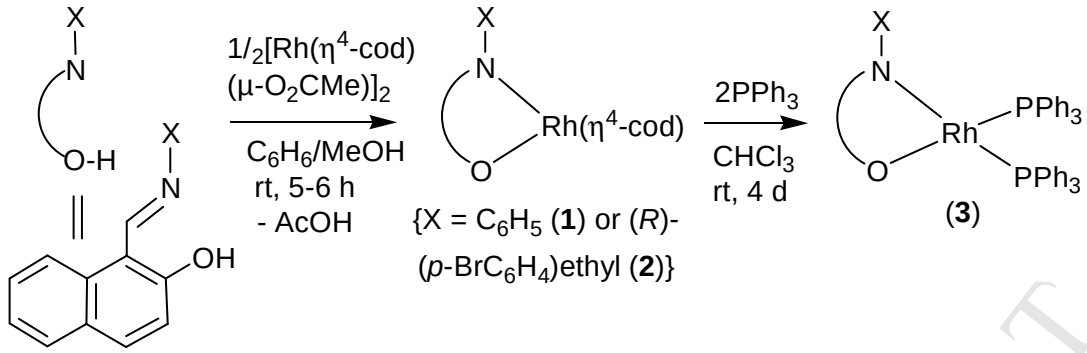

Scheme 1. Synthetic route to the formulation of the compounds **1** - **3**.

3.2. Mass spectra

Mass spectra of the compounds (Figure 1, S1) show the molecular ion peaks at *m*/*z* 457 $[M]^+$ (**1**), 586/602 $[M+Na/K]^+$ (**2**), and 994 $[M(O)]^+$ (**3**), confirm the formation of the compounds as depicted in the reaction Scheme 1. The spectra further show several ion peaks for $[Rh(SB)]^+$ (SB = deprotonated Schiff base), $[HSB]^+$, and fragmented Schiff base ligands. Compound **3** is very sensitive to air and forms the oxidative adduct of $[M(O)]^+$ while running the spectra. The spectrum further shows several ion peaks for $[M–PPh_3]^+$, $[M–PPh_3+K]^+$, $[Rh(SB2)+Na/K]^+$ and oxidized triphenylphosphine $[(PPh_3O)_n+H/Na/K]^+$ (n = 1, 2, 3) (Figure 1), which are further supported by ^{31}P NMR spectra discussed below.

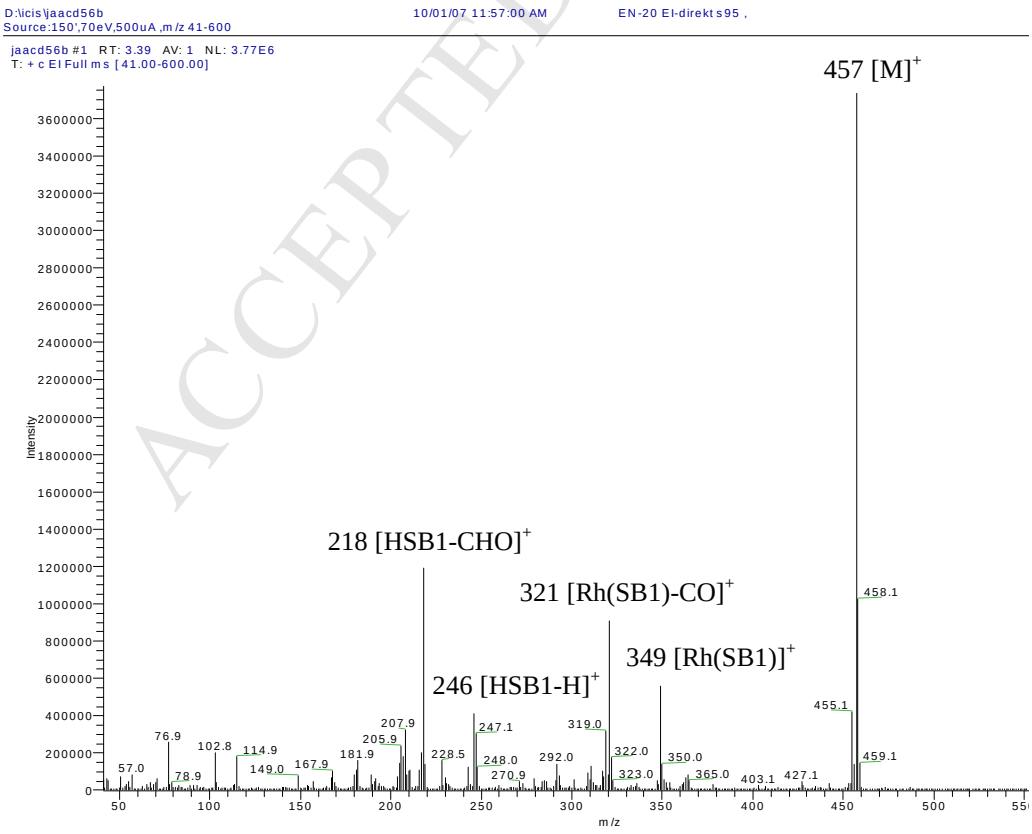

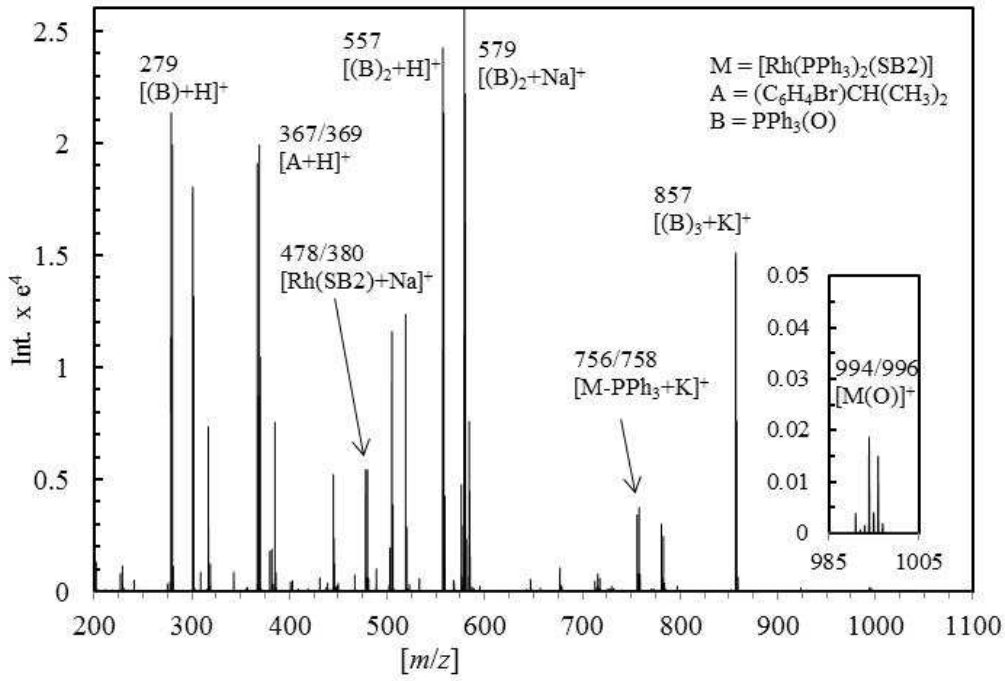

Fig. 1. EI and ESI mass spectra of compounds **1** (top) and **3** (bottom), respectively.

3.3. Solid state X-ray structure

Complex **1** has the 2-oxo-1-naphthaldiminato ligand coordinated with six-membered Rh-*N,O*-chelate ring formation and the rhodium-bound η^4-cod fragment (Figure 2) in distorted square planar geometry. The bond lengths and angles are listed in Table 2, comparable as seen before in the analogous Rh{*N,O*}(η^4-cod) complexes with {*N,O*} = salicylaldiminato/naphthaldiminato Schiff base ligands [8,11,13]. From the aromatic rings in the complexes there are no detectable π-π interactions [22], but intermolecular C-H$\cdots\pi$ contacts [23] are evident in the packing; a detailed analysis is reported in the Supporting Information.

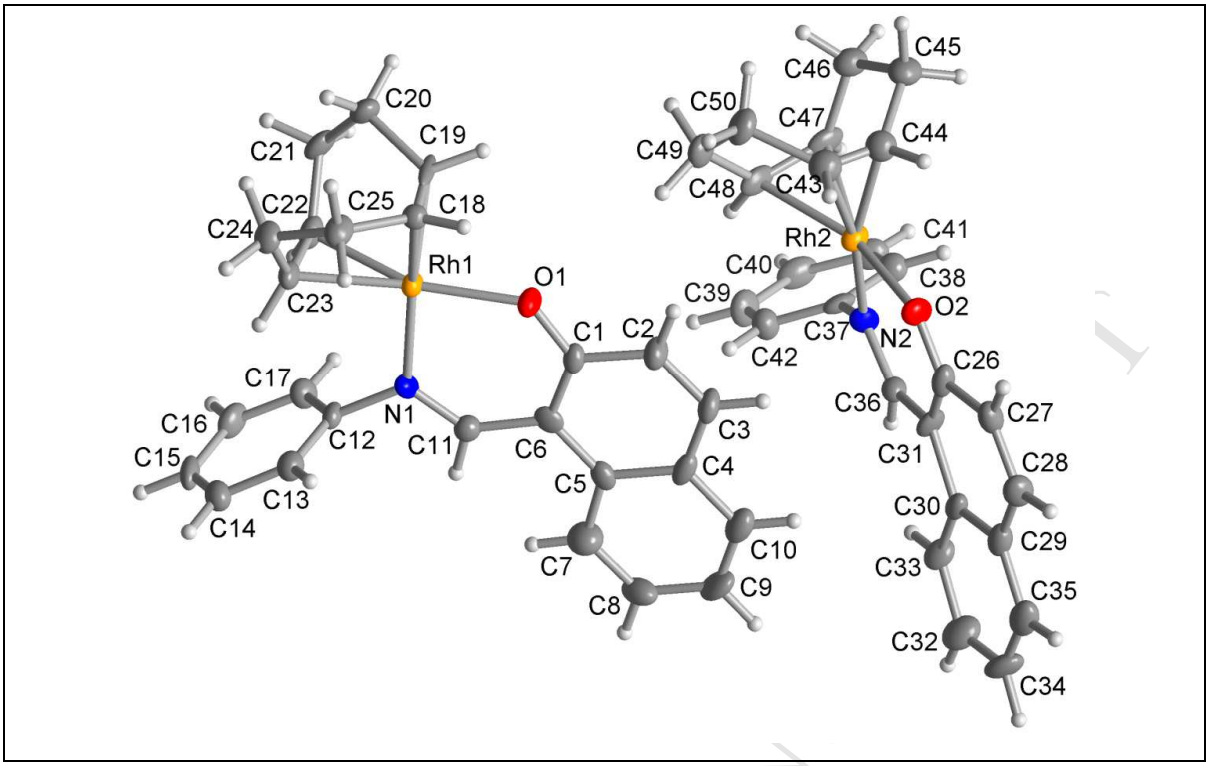

Fig. 2. Thermal ellipsoid plot (50% level) for compound **1**; bond lengths and angles are listed in Table 1.

Compound **1**			Compound **2**	
X-ray (Molecule **A)**	X-ray (Molecule **B)**	Opt.	X-ray [a]	Opt.

Table 2

Selected bond lengths [Å] and angles [°] in X-ray and optimized structures for compounds **1** and **2**.

Compound **1**						Compound **2**		
X-ray (Molecule **A**)		X-ray (Molecule **B**)		Opt. Str.			X-ray [a]	Opt. Str.
Rh1–O1	2.029(5)	Rh2–O2	2.042(5)	Rh–O	2.0396	Rh–O	2.028(2)	2.034
Rh1–N1	2.075(7)	Rh2–N2	2.048(7)	Rh–N	2.0856	Rh–N	2.073(3)	2.085
Rh1–C18	2.094(8)	Rh2–C43	2.109(10)	Rh–C18	2.1737	Rh–C20	2.146(3)	2.202
Rh1–C19	2.126(8)	Rh2–C44	2.091(9)	Rh–C19	2.1948	Rh–C21	2.130(3)	2.180
Rh1–C22	2.108(8)	Rh2–C47	2.129(8)	Rh–C22	2.1520	Rh–C24	2.111(3)	2.169
Rh1–C23	2.121(8)	Rh2–C48	2.108(8)	Rh–C23	2.1784	Rh–C25	2.111(3)	2.156
O1–Rh1–N1	89.1(2)	O2–Rh2–N2	89.0(2)	O–Rh–N	88.40	C-Br	1.898(4)	1.964
O1–Rh1–C18	88.0(3)	O2–Rh2–C43	90.4(3)	O–Rh–C18	85.93	O–Rh–N	88.87	88.74
O1–Rh1–C19	88.5(3)	O2–Rh2–C44	88.3(3)	O–Rh–C19	87.57	O–Rh–C20	87.86(12)	87.10
O1–Rh1–C22	155.5(3)	O2–Rh2–C47	161.6(3)	O–Rh–C22	156.30	O–Rh–C21	86.47(15)	85.34
O1–Rh1–C23	164.3(3)	O2–Rh2–C48	158.8(3)	O–Rh–C23	162.97	O–Rh–C24	162.12(12)	162.26
N1–Rh1–C18	156.5(3)	N2–Rh2–C43	168.7(3)	N–Rh–C18	158.02	O–Rh–C25	157.44(12)	156.37
N1–Rh1–C19	169.7(4)	N2–Rh2–C44	161.8(3)	N–Rh–C19	162.93	N–Rh–C20	166.14(13)	164.21
N1–Rh1–C22	95.7(3)	N2–Rh2–C47	96.2(3)	N–Rh–C22	96.06	N–Rh–C21	155.05(11)	156.80
N1–Rh1–C23	95.5(3)	N2–Rh2–C48	94.5(3)	N–Rh–C23	99.24	N–Rh–C24	96.42(12)	99.09
						N–Rh–C25	96.49(12)	96.99

[a] from ref [12]; Opt. Str. = optimized structure.

There are two symmetry-independent molecules in the asymmetric unit, that is, molecule A with Rh1 and molecule B with Rh2 centre. The structures of the analogous Ni/Cu/Zn(II)-complexes with *R*/*S*-N-1-(Ar)ethyl-2-oxo-1-naphthaldiminate (Ar = C_6H_5 or *p*-C_6H_4OMe) also contained two symmetry-independent molecules [24,25,26]. Two symmetry-independent molecules, that is, two identical chemical formula units in the structural asymmetric unit [27] give a Z' = 2 structure. The definition of Z' refers to the number of formula units in the unit cell (here 8) divided by the number of independent general positions (here 4) [28]. Such Z' > 1 structures [29] can derive from a metastable structure, that is, a crystal "on the way", [27-29, 30] or from strong and special supramolecular (e.g. hydrogen bonding) interactions between the two (or more) symmetry-independent units [31]. A molecule with different equi-energetic conformations also gives a high Z' such that these conformations co-exist in the crystal [32]. Here, in the Rh structure **1** the conformational difference between the symmetry-independent molecules is nearly insignificant. The two symmetry-independent molecules are quite superimposable (Figure 3). These very small deviations do not appear to justify the presence of two symmetry-independent molecules.

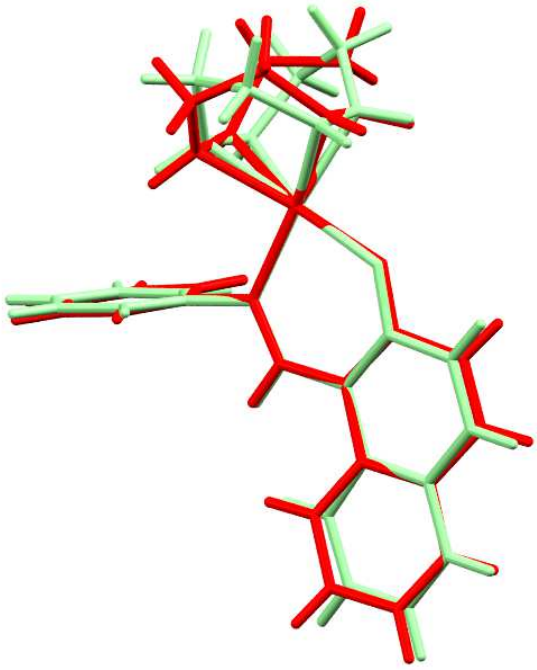

Fig. 3. Overlay of the two symmetry independent molecules A and B in **1**. The Rh1 molecule is shown in green, while Rh2 molecule in red. Three atoms RhNO were specified to orient the overlay which was managed with the "Molecule overlay" option in Mercury 3.8 (copyright CCDC 2001-2016, http://www.ccdc.cam.ac.uk/mercury/).

Thus, the rationalization of the Z' = 2 structure must be sought for in the packing arrangement. Each independent molecule in **1** is arranged in layers composed of molecules of the same kind (Figure 4). These layers lie parallel to the *bc* plane and stack alternately for the independent molecules along the *a* direction. Even if the CH-π interactions between the Rh1 and Rh2 molecules appear rather weak supramolecular interactions (see listing of CH-π interactions and Figure S1 in Supporting Information).

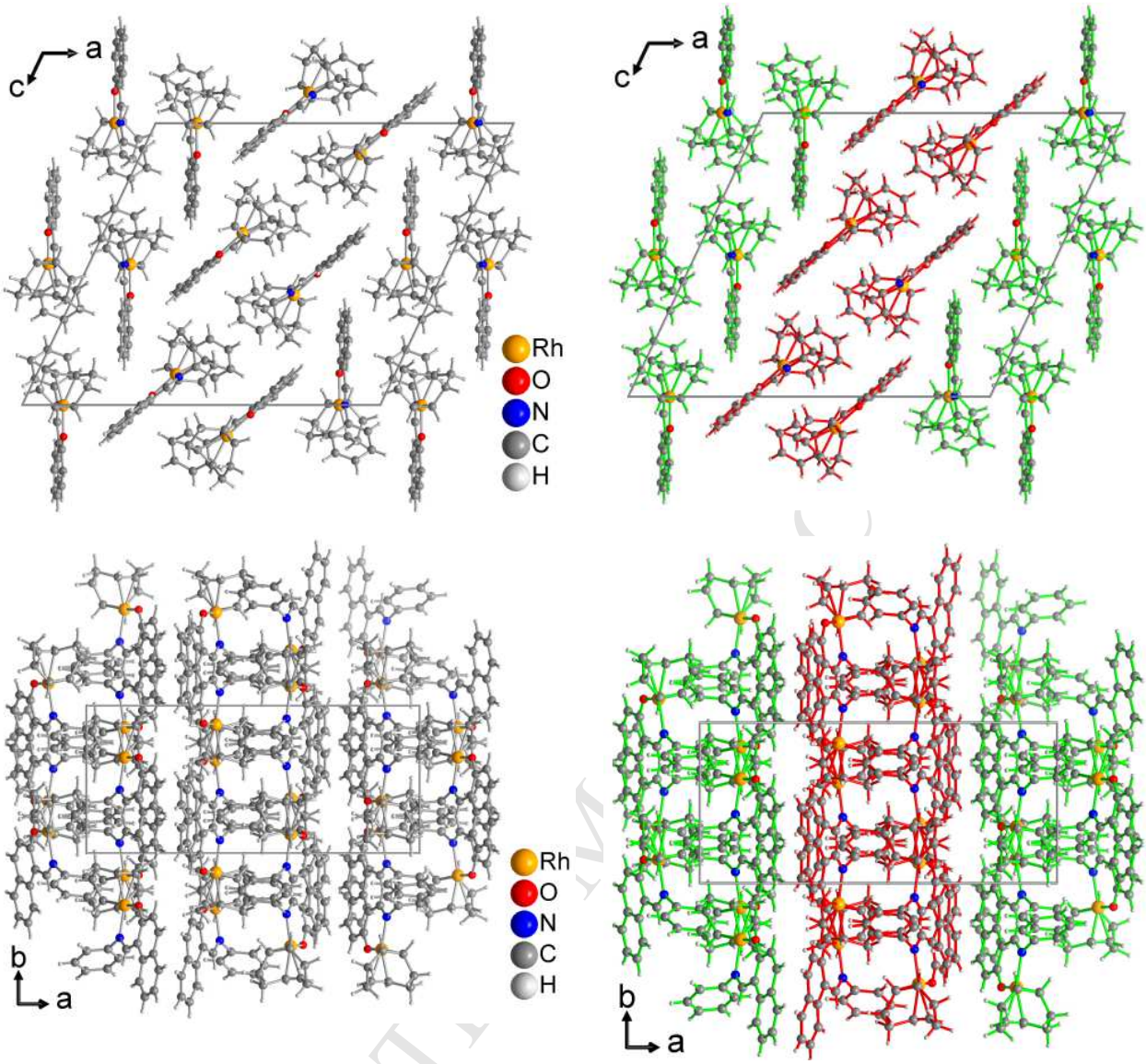

Fig. 4. Packing diagrams for **1** with projection on two different planes. The Rh1 molecules are shown in green, and Rh2 molecules in red.

3.4. Optimized structures and vibrational spectra

The optimized structures by DFT, calculated at B3LYP/SDD, based on the X-ray data for compounds **1** and **2** are shown in Figure 5. The experimental and calculated bond lengths and angles are comparable (Table 2). Experimental vibrational spectra show several characteristics bands mainly for the coordinated Schiff base ligand at the range of 3055-2922, 1615 - 1602 and 1584 - 1533 cm^{-1}, associated with the νC–H, νC=N and νC=C, respectively (Figure S2 and Table 3) [10-14,15]. The computed vibrational spectra show these bands at compareable range (Figure S3 and Table 3). The spectra taken as KBr disc show a strong broad band at 3449 cm^{-1} due to νH_2O from KBr, which is obviously absent in the ATR spectra (Figure S2).

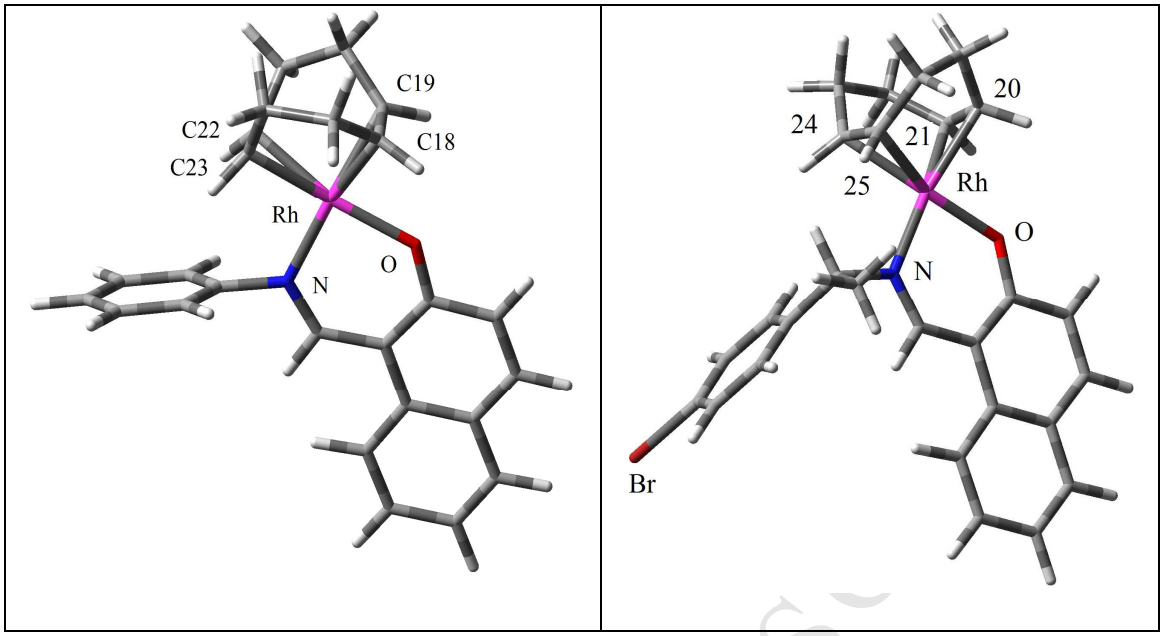

Fig. 5. Optimized structures, calculated at B3LYP/SDD, for compounds **1** and **2**.

Table 3.

Experimental and calculated (at B3LYP/SDD) vibrational spectra of **1** and **2** at ambient temperature.

Entity	νC–H[a]	νC=N[a]	νC=C[a]
1[b]	3042, 3007, 2958, 2922w (3220, 3180, 3100, 3060, 3004s)	1615, 1602vs (1668, 1612vs)	1575, 1534vs (1572, 1516vs)
2[c]	3055, 3010, 2950w (3220, 3140, 3100, 3060, 3004s)	1611, 1602vs (1668, 1612vs)	1584, 1533vs (1580, 1516vs)
3[b]	3060, 3030, 3006, 2940w	1614, 1606vs	1588, 1537vs

[a] Values in parentheses correspond to the computed spectra; [b] spectra taken as KBr dics; [c] ATR spectra.

3.5. ^{1}H NMR spectra

In ^{1}H NMR spectra (Figure **6** and Table **4**), the rhodium coordinated 1,5-cyclooctadiene shows different multiplets for the exo- and endo-methylene protons {i.e., C*H*$_2$(cod)$_{exo}$ and C*H*$_2$(cod)$_{endo}$} and olefin protons {C*H*(cod)} [5-11,33,34]. The exo- and endo-methylene protons show a multiplet in each at δ 1.77 and 2.42 ppm in **1** and δ 2.01 and 2.56 ppm in **2**, respectively. The four olefin protons show two doublets at δ 3.30 (J = 2.6 Hz) and 4.61 ppm (J = 2.4 Hz) in **1** and δ 3.87 (J = 7.0 Hz) and 4.67 (J = 7.5 Hz) ppm in **2**. The presence of two boublets for olefin protons is explained by the *trans effects* of the coordinated *N*,*O*-chelate ligand on the proton resonances [5-11,33]. It has been reported that two kinds of olefin protons resonances (i.e., giving two boublets) arise from two sets

of two equivalent protons *trans* to *N* (downfielded peak) and *trans* to *O* atom (upfielded peak), respectively. This result reflects the asymmetric nature of the olefin protons. However, the rhodium coordinated Schiff base ligand shows a doublet at δ 1.74 ppm (J = 6.8 Hz) and a quartet at δ 4.46 ppm (J = 6.6Hz) for the methyl and methine protons, respectively in **2**. The imine proton (C*H*N) shows a doublet at δ 8.88 ppm (J = 2.0 Hz) in **1** and a singlet at δ 8.87 ppm in **2**, the doublet is due to ^{103}Rh–^{1}H coupling [1-3,8,10-12].

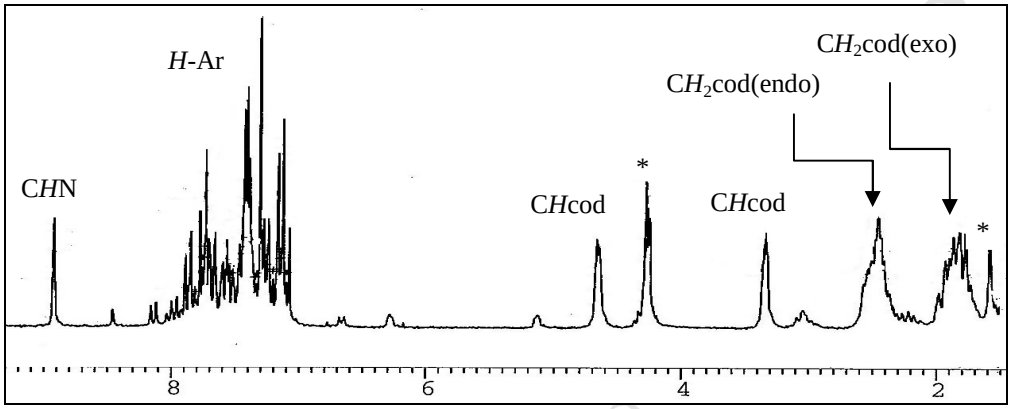

Fig. 6. ^{1}H NMR (400 MHz, δ/ppm) spectra of compound **1** in $CDCl_3$ at 20 ^{o}C (asterisked are due to solvent).

Table 4

^{1}H NMR data (400 MHz, δ/ppm) of compounds **1-3** in $CDCl_3$ at 20 ^{o}C [a].

Compound	$CH_2(cod)_{exo}$	$CH_2(cod)_{endo}$	CH(cod)	CH	CH_3	CHN
1[*]	1.77 (m, 4H)	2.42 (m, 4H)	3.30 (m, 2H), 4.61 (m, 2H)	-	-	8.88 (d, J = 2.0Hz, 1H)
2	1.93 (m, 2H), 2.01 (m, 2H)	2.45 (m, 2H), 2.63 (m, 2H)	3.85 (m, 2H), 4.64 (m, 2H)	4.46 (q, J = 6.6Hz, 1H)	1.74 (d, J = 6.7 Hz, 3H)	8.87 (d, J = 2.0Hz, 1H)
3	-	-	-	4.3 (m, 1H)	1.85 (m, 3H)	8.45 (s, 1H)

[a] Aromatic protons peaks are listed in the experimental section; [*]spectra run on 200 MHz Spectrometer.

3.6. ^{31}P NMR spectra

The reaction progress was monitored by taking ^{31}P NMR spectra (Figure 7, Table 5) after 4 h, 24 h and 4 days, respectively. The spectra show the formation of a mixture products of $[Rh(PPh_3)_4]^+$, $[Rh(\eta^4\text{-cod})(PPh_3)_2]^+$, and $PPh_3(O)$ even after 24 h of reaction. The former two compounds show two doublets at δ 12.94 ppm ($J_{P\text{-}Rh}$ = 77 Hz) and 30.83

ppm ($J_{P\text{-}Rh}$ = 150 Hz), respectively. While the latter one shows a singlet at δ 29.56 ppm. In $[Rh(PPh_3)_4]^+$, four P-atoms coordinate to the rhodium atom in an uniform environment, resulting the formation of a doublet. Similarly, two P-atoms coordinate to the rhodium atom which is further bonded to the four equvelent olefin carbon atoms in $[Rh(\eta^4\text{-cod})(PPh_3)_2]^+$ and results in a doublet. However, the compound $[Rh(PPh_3)_2(SB2)]$ (**3**), isolated after 4 days, shows two doublets at δ 38.59 ($J_{P\text{-}Rh}$ = 124Hz) and 39.55 ppm ($J_{P\text{-}Rh}$ = 153Hz) (Figure 7), assigned for two P-atoms coordinated to the rhodium *trans* to *N* and *trans* to *O* atoms, respectively [10]. The spectrum further shows peaks for $PPh_3(O)$ and $[Rh(PPh_3)_4]^+$. As discussed above, compound **3** is very sensitive to air and easily decomposes to form the oxidized triphenylphosphine while preparing the sample for running the spectra. In addition, very little amount of $[Rh(PPh_3)_4]^+$ is yet present in the sample though the product is repeatedly washed.

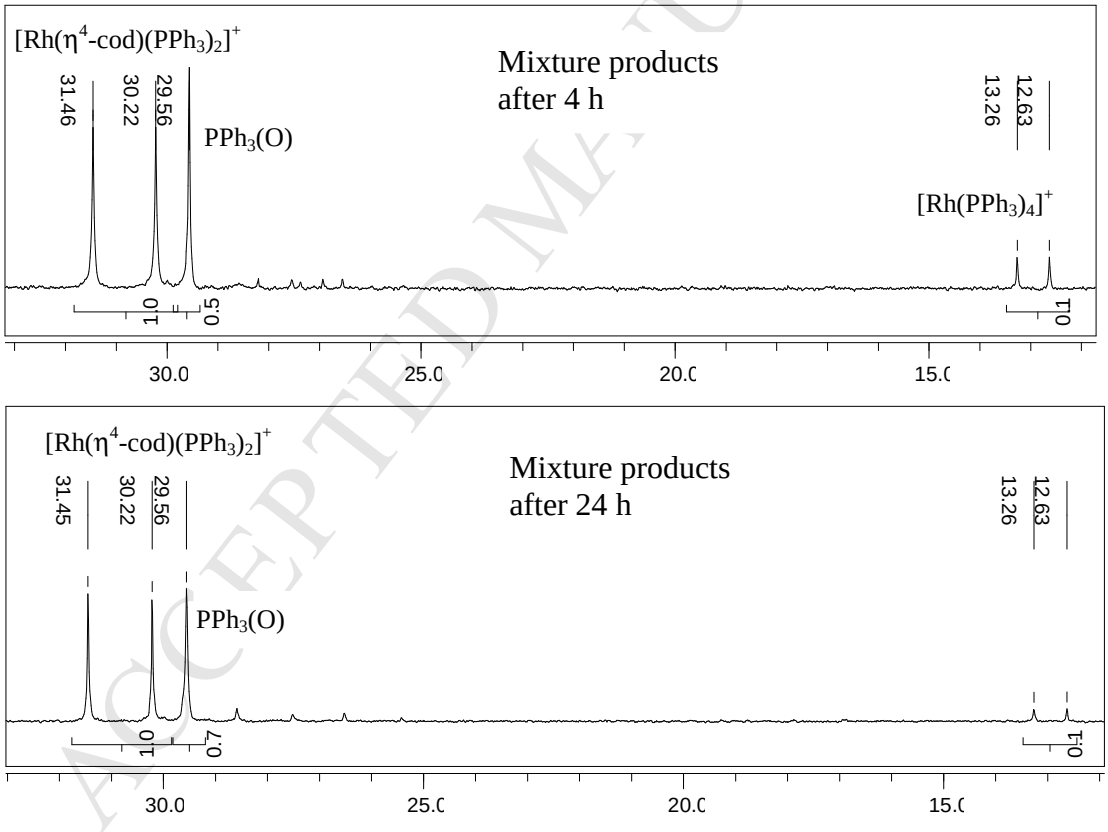

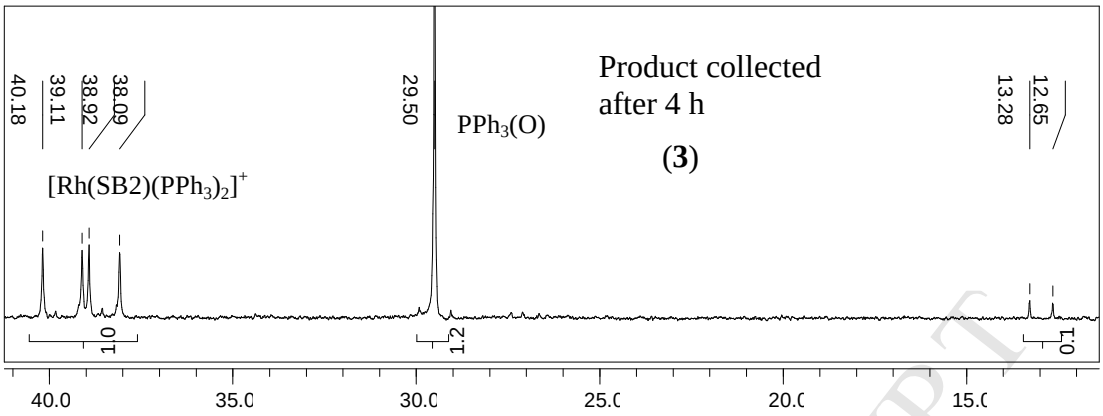

Fig. 7. ^{31}P NMR spectra of mixture products in course of reaction, and the compound **3** in $CDCl_3$ at 20 ^{o}C.

Table 5.

^{31}P NMR data (121.5 MHz, δ/ppm) of compound **3** in $CDCl_3$ at 20 ^{o}C.

Prod.	$[Rh(PPh_3)_2(SB2)]$ (**3**)	$[Rh(PPh_3)_4]^+$	$PPh_3(O)$	$[Rh(\eta^4\text{-cod})(PPh_3)_2]^+$
4h [a]	-	12.94 (d, $J_{P\text{-}Rh}$ = 77Hz)	29.56 (s)	30.83 (d, $J_{P\text{-}Rh}$ = 150 Hz)
24h [a]	-	12.94 (d, $J_{P\text{-}Rh}$ = 77Hz)	29.55 (s)	30.83 (d, $J_{P\text{-}Rh}$ = 150 Hz)
4d [b]	38.59 (d, $J_{P\text{-}RhN}$ = 124 Hz) 39.55 (d, $J_{P\text{-}RhO}$ = 153 Hz)	12.96 (d, $J_{P\text{-}Rh}$ = 77Hz)	29.49 (s)	-

[a] Mixture products in course of reaction, [b] Product collected after 4 days.

3.7. Thermally induced structural phase transformation

Thermally induced structural phase transformation has been reported for the transition metal-*N*,*O*-chelate complexes which accompanying a change from low temperature crystalline phase at distorted square planar/tetrahedral to high temperature isotropic liquid phase at regular square planar/tetrahedral geometry [9,21,24-26,35,36]. Differential Scanning Calorimetry (DSC) has successfully been used to study the phenomenon. DSC heating curve (Figure 8) shows a peak at *ca.* 237 (ΔH = – 17.14 kJ/mol for **1**) and 200 ^{o}C (ΔH = – 24.17 kJ/mol for **2**), associated to the structural phase transformation. On the other hand, cooling curve shows no corresponding peak on the reverse direction. The result indicates an irreversible phase transformation from crystalline to isotropic liquid phase.

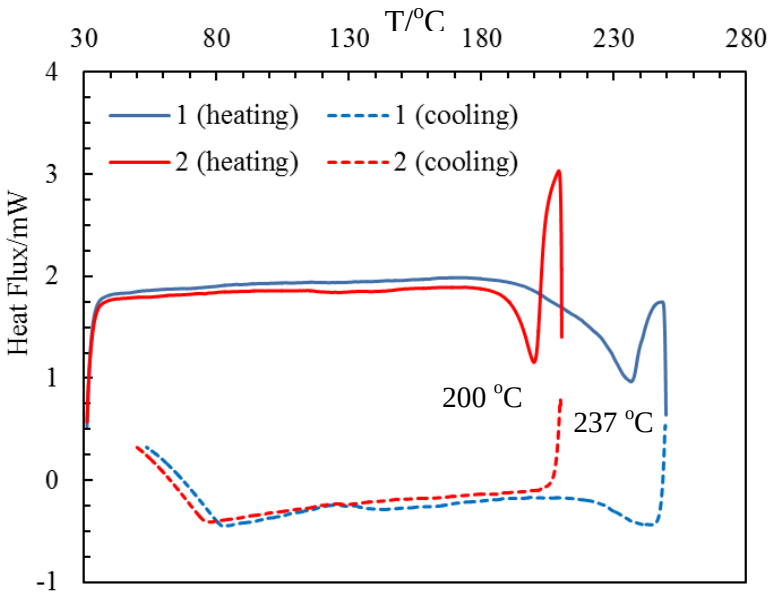

Fig. 8. DSC analyses curves for compounds **1** and **2**.

3.8. Electronic spectra and TDDFT calculations

Electronic spectra of the compounds in chloroform (Figure 9) feature several strong bands/shoulders below 300 nm, associated with the intra-ligand $\pi\rightarrow\pi^*/n\rightarrow\pi^*$ transitions (LLCT). The spectra further show a medium broad band at 300 - 350 nm (λ_{max} = 324 nm), and a weak broad band at 350 - 460 nm (λ_{max} = 418 for **1**, and 414 nm for **2**), assigned to the metal-ligand charge transfer (MLCT) transitions based on the formation of Rh(η^4-cod)$^+$ and Rh(naphthaldiminate) species, respectively [5-12,33]. Computed spectra by TDDFT, calculated at B3LYP/SDD, are comparable to the experimental spectra (Figure 9 and Table 6). A straightforward assignment, however, on computed spectra is hampered by the complexity of the system and the presence of a large number of excitations at a single wave length [9,21,25-27]. Thus, we report herein only the selected and simplified transitions with their assignments relevant to the experimental data (i.e., those transitions contributing most to the spectra) (Table 6). The assignments reveal that the several metal-centered transitions occur deeply in the UV region, where the ligand-centered transitions usually occur. Although the d-d transitions are not allowed in Rh(I), the distortion from square-planar geometry and coupling of the σ-type ligand orbitals with the metal d-orbitals exhibit the metal-centered d-d excitation [9,21]. Hence a combined metal-metal (M-M) and metal-ligand (M-L) transitions bands appear with λ_{max} at 411 (**1**) and 402 nm (**2**) with the highest molecular orbitals (MOs) contributions of *ca.* 81% for HOMO-1 to LUMO transitions in each. Similarly, a combined M-M, M-L and ligand-ligand (L-L) bands

appear with λ_{max} = 348 (**1**) and 340 nm (**2**) with high MOs contributions of *ca.* 56 and 49% for HOMO-2 to LUMO transitions, respectively. These two bands including several other computed bands are very close to the experimental bands/shoulders (Figure 9 and Table 6). The HOMOs-1 and LUMOs for both compounds are presented in Figure 10.

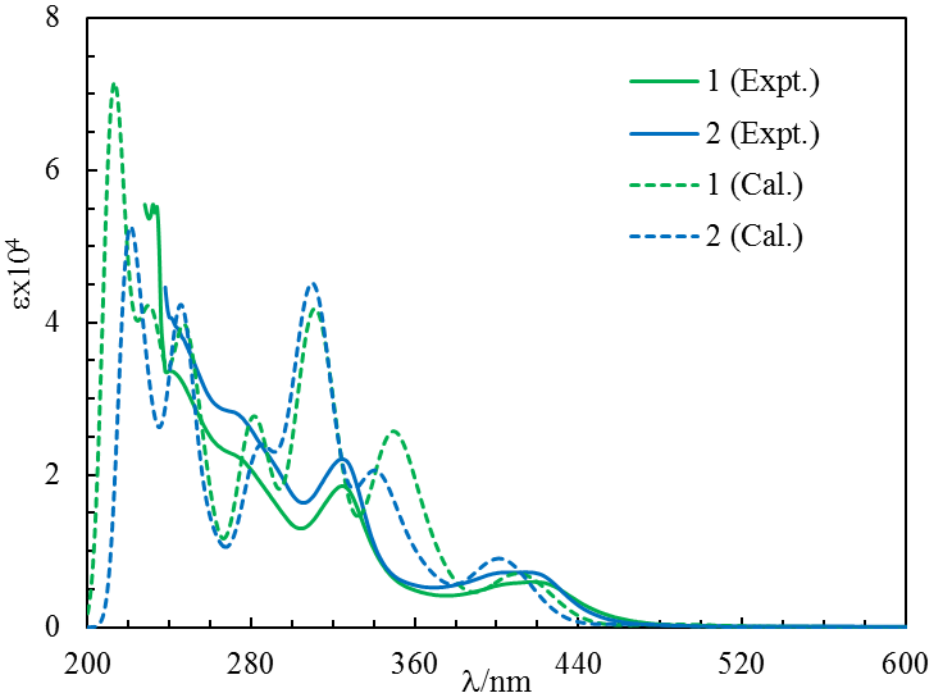

Fig. 9. Experimtal and calculated (at B3LYP/SDD) electronic spectra of **1** and **2** in chloroform at 20 ^{o}C.

Table 6.

Selected excitation properties, calculated at B3LYP/SDD level of theory, for **1** and **2** in chloroform.

Wavelength (nm) [#]	Oscillator Strength (f)	MOs Contributions (%) [a]	Assignments [b]
		Compound **1**	
411 (418)	0.0683	H-1→L (81), H→L+2 (6)	M-M, M-L
367	0.0468	H-3→L (57), H-2→L (36)	M-M, M-L
348 (324)	0.2299	H-3→L (36), H-2→L (56)	M-M, M-L,L-L
310	0.2517	H-1→L+1 (57)	M-M, ML, L-L
280 (~270sh)	0.0899	H-1→L+3 (86)	M-M, M-L, L-L
248	0.1561	H-3→L+4 (11), H-1→L+5 (18)	M-M, M-L, L-L
233 (~234sh)	0.1466	H-5→L+1 (15), H-2→L+5 (23)	M-L, L-L
215	0.2433	H-4→L+5 (18), H-7→L+2 (11)	ML, LM, L-L
		Compound **2**	
402 (414)	0.0871	H-1→L (81), H→L+6 (11)	M-M, M-L

370	0.0269	H→L+2 (19), H→L+6 (41)	M-M, M-L
340 (324)	0.1841	H-3→L (41), H-2→L (49)	M-M, M-L, L-L
308	0.2199	H-1→L+1 (76)	M-M M-L, L-L
283 (~270sh)	0.1053	H-1→L+4 (9), H-1→L+5 (73)	M-M, M-L, L-L
247	0.1051	H-3→L+2 (10), H-3→L+3 (36)	M-M, M-L, L-L
244 (~240sh)	0.1214	H-9→L (19), H-3→L+3 (36)	M-M, M-L, L-L
220	0.1391	H-6→L+2 (17), H-5→L+5 (13)	M-L, L-M, L-L
217	0.1312	H-7→L+3 (46), H-7→L+6 (16)	L-M, L-L

[#] Experimental values in parentheses; [a] H/L = HOMO/LUMO; [b] M-M = metal d-d, M-L/L-M = metal-ligand/ligand-metal, L-L= ligand-ligand transitions.

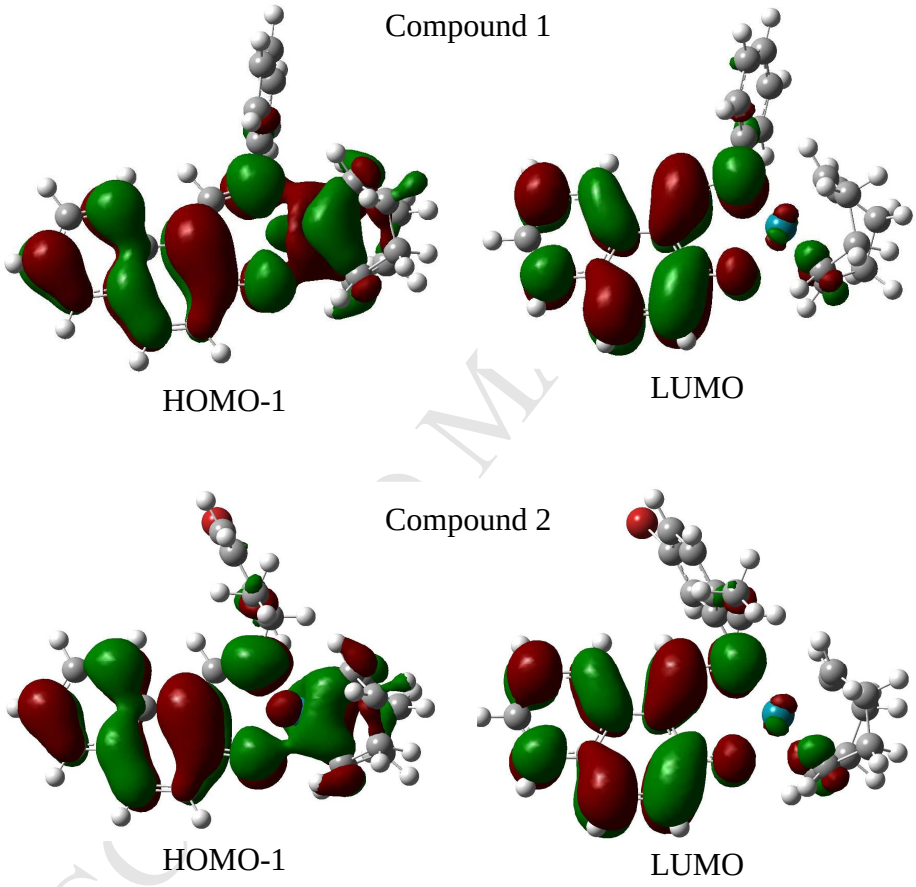

Fig. 10. HOMOs-1 and LUMOs, calculated at B3LYP/SDD level of theory, for compounds **1** and **2** in chloroform.

Electronic spectra of **1** in different solvents (Figure S5 and Table 7) demonstrate that both the absorption maxima (λ_{max}) and band intensities (ε_{max}) change with the solvents' nature [9,37,38,39]. Thus a negative solvatochromic trend is envisioned with shifting λ_{max} to the higher energies (blue shift) in the solvents of increasing dielectric constants (ε) and Gutmann's Acceptor (AN) number [40], respectively (Figure 11).

Table 7.

Electronic spectral data of compound **1** in different solvents at 20 ^{o}C.

Solvent [a]	$\pi\rightarrow\pi^*/n\rightarrow\pi^*$: LLCT ($\lambda_{max}/\varepsilon_{max}$) [b]	Rh(η^4-cod)$^+$: MLCT ($\lambda_{max}/\varepsilon_{max}$) [b]	Rh(SB): MLCT ($\lambda_{max}/\varepsilon_{max}$) [b]
1			
MeOH (0.018)	<300 (226/23888)	300-350 (321/5778)	360-500 (415/2306)
EtOH (0.025)	<300 sh	300-350 (322/8280)	360-500 (417/3140)
AC (0.023)	-	-	360-500 (416/7196)
C_6H_6 (0.025)	<300 sh	300-350 (324/24940)	360-500 (420/8380)
C_6H_{14} (0.025)	<300 sh	300-350 (322/21320)	360-500 (421/6900)
DCM (0.025)	<300 sh	300-350 (323/24100)	360-500 (417/7820)
$CHCl_3$ (0.025)	<300 sh	300-350 (324/18520)	360-500 (418/5940)
EtOAc (0.026)	<300 sh	300-350 (321/28288)	360-500 (417/9423)
2			
$CHCl_3$ (0.026)	<300 sh	300-350 (324/22077)	330-430 (414/7212)

[a] Concentration in parentheses in mM·L^{-1}; [b] λ_{max} in nm, ε_{max} in L·mM^{-1}·dm^{-3}; SB = deprotonated Schiff base ligands.

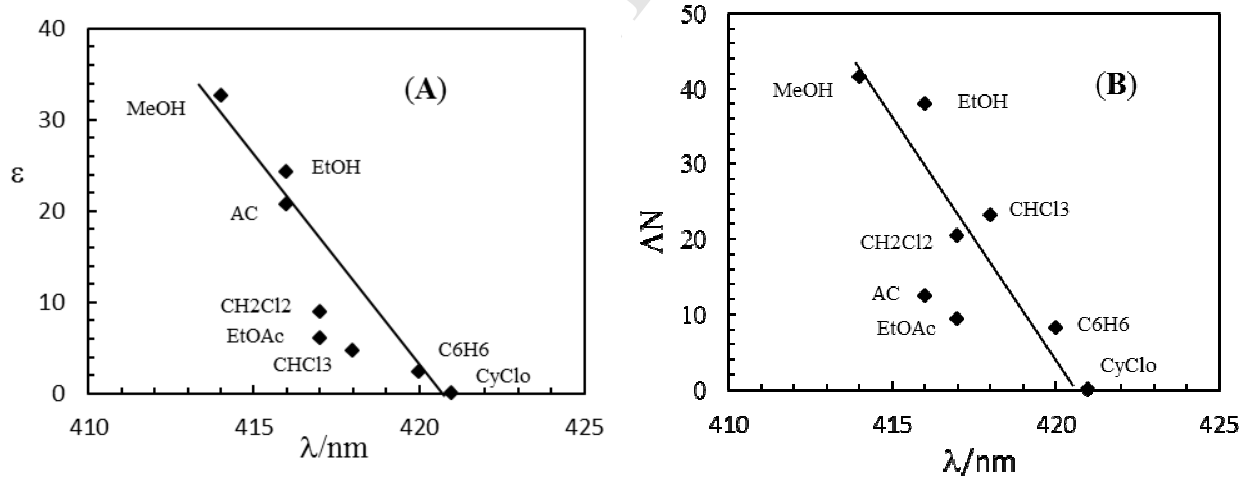

Fig. 11. Changes of absorption maxima (λ_{max}/nm) with (**A**) Dielectric constant (ε) and (**B**) Acceptor number (AN) of the solvents for **1** at 20 °C, respectively.

4. Conclusion

Rh(η^4-cod)-Schiff base complexes are formed *via* coordination of 2-oxo-1-naphthaldiminate ligand to the Rh(η^4-cod)-fragment in distorted square planar geometry. The structure consists of two symmetry-independent molecules (**A** and **B**) in the asymmetric unit to give a Z' = 2 structure. The optimized geometry and excitation

properties calculated by DFT/TDDFT are comparable to the experimental results. In ^{1}H NMR spectra, rhodium coordinated cod ligand shows two multiplets for the exo- and endo-methylene protons, respectively. While the olefin protons show two doublets due to *trans effects* of the coordinated *N,O*-chelate ligand on the proton resonances. ^{31}P NMR spectra demonstrate two sets of doublets for two assymetic P-atoms bound to the Rh(I) *trans* to *N* and *O* atoms, respectively. An irrversibel phase transformation from crystalline to isotropic liquid phase is revealed by DSC analyses. The present results will certainly be useful in understanding the syntheses, reactivities and cataltic behaviors of Rh(I)-*N,O*-chelate Schiff base complexes.

Acknowledgements

We acknowledge the"Wazed Miah Science Research Centre"at Jahangirnagar University, Dhaka, Bangladesh for obtaining elemental data. Our sincere thank to Professor KS. Hagen, Department of Chemistry, Emory University, for X-ray measurement of compound **1**. For computational resource, we thank to Professor ABP Lever, Department of Chemistry, York University, Toronto, and the *Shared Hierarchical Academic Research Computing Network* (SHARCNET: www.sharcnet.ca) Ontario, Canada.

References

[1] (a) N. Platzer, N. Goasdoue, R. Bonnaire, J. Organomet. Chem. 160 (1978) 455;

(b) R. Bonnaire, C. Potvin, J.M. Manoli, Inorg. Chim. Acta 45 (1980) L255;

(c) R. Bonnaire, J.M. Manoli, C. Potvin, N. Platzer, N. Goasdoue, D. Davoust, Inorg. Chem. 21 (1982) 2032;

(d) J.G. Leipoldt, E.C. Grobler, Inorg. Chim. Acta 72 (1983) 17;

(e) A.P. Martinez, M.P. Garcia, F.J. Lahoz, L.A. Oro, Inorg. Chem. Commun. 5 (2002) 245.

[2] (a) H. Brunner, H. Leyerer, J. Organomet. Chem. 334 (1987) 369;

(b) A. Rogers, B.O. West, J. Organomet. Chem. 70 (1974) 445;

(c) R.J. Cozens, K.S. Murray., B.O. West, J. Organomet. Chem. 27 (1971) 399;

(d) R. Ugo, G.L. Monica, S. Cenini, F. Bonati, J. Organomet. Chem. 11 (1968) 159.

[3] (a) H. Brunner, H. Fisch, J. Organomet. Chem. 335 (1987) 1;

(b) H. Brunner, G. Riepl, Angew. Chem. 94 (1982) 369;

(c) H. Brunner, B. Reiter, G. Riepl, Chem. Ber. 117 (1984) 1330;

(d) M.E. Wright, S.A. Svejda, A.M. Arif, Inorg. Chim. Acta 175 (1990) 13.

[4] (a) M.D. Jones, M.F. Mahon, J. Organomet. Chem. 693 (2008) 2377;

(b) G. Zassinovich, F. Grisoni, J. Organomet. Chem. 247 (1983) C24;

(c) V.A. Pavlov, M.G. Vinogradov, E.V. Starodubtseva, G.V. Cheltsova, V.A. Ferapontov, O.R. Malyshev, G.L. Heise, Russ, Chem, Bull, Intl, Ed. 50 (2001) 734.

[5] M. Enamullah, M. Hasegawa, T. Hoshi, J. Okubo. J. Bangladesh Chem. Soc. 18 (2005) 165.

[6] M. Enamullah, A. Sharmin, M. Hasegawa, T. Hoshi, A.-C. Chamayou, C. Janiak. Eur. J. Inorg. Chem. (2006) 2146.

[7] M. Enamullah, A.K.M. Royhan Uddin, M. Uddin. J. Bangladesh Chem. Soc. 21 (2008) 128.

[8] C. Janiak, A.-C. Chamayou, A.K.M. Royhan Uddin, M. Uddin, K.S. Hagen, M. Enamullah. Dalton Trans. (2009) 3698.

[9] M. Enamullah, M.K. Islam, M.A. Halim, C. Janiak. J. Mol. Str. 1099 (2015) 154.

[10] M. Enamullah, M. Uddin, W. Linert. J. Coord. Chem. 60 (2007) 2309.

[11] M. Enamullah, A.-C. Chamayou, C. Janiak. Z. Naturforsch. 62b (2007) 807.

[12] M. Enamullah, A.K.M. Royhan Uddin, G. Hogarth, C. Janiak. Inorg. Chim. Acta 387 (2012) 173.

[13] M. Enamullah. J. Coord. Chem. 64 (2011) 1608.

[14] M. Enamullah. J. Coord. Chem. 65 (2012) 911.

[15] SMART, Data Collection Program for the CCD Area-Detector System; SAINT, Data Reduction and Frame Integration Program for the CCD Area-Detector System. Bruker Analytical X-ray Systems, Madison, Wisconsin, USA, 1997.

[16] G. Sheldrick, Program SADABS: Area-detector absorption correction, University of Göttingen, Germany, 1996.

[17] G.M. Sheldrick, SHELXS-97, SHELXL-97, Programs for Crystal Structure Analysis, University of Göttingen, Germany, 1997.

[18] DIAMOND 3.0e for Windows. Crystal Impact Gbr, Bonn, Germany; http://www.crystalimpact.com/diamond.

[19] H.D. Flack, Acta Crystallogr. A 39 (1983) 876.

[20] Gaussian 09, Revision D.01, M.J. Frisch, G.W. Trucks, H.B. Schlegel, G.E. Scuseria, M.A. Robb, J.R. Cheeseman, G. Scalmani, V. Barone, B. Mennucci, G.A. Petersson, H. Nakatsuji, M. Caricato, X. Li, H.P. Hratchian, A.F. Izmaylov, J. Bloino, G. Zheng, J.L. Sonnenberg, M. Hada, M. Ehara, K. Toyota, R. Fukuda, J. Hasegawa, M.

Ishida, T. Nakajima, Y. Honda, O. Kitao, H. Nakai, T. Vreven, J.A. Montgomery, Jr., J.E. Peralta, F. Ogliaro, M. Bearpark, J.J. Heyd, E. Brothers, K.N. Kudin, V.N. Staroverov, R. Kobayashi, J. Normand, K. Raghavachari, A. Rendell, J.C. Burant, S.S. Iyengar, J. Tomasi, M. Cossi, N. Rega, J.M. Millam, M. Klene, J.E. Knox, J.B. Cross, V. Bakken, C. Adamo, J. Jaramillo, R. Gomperts, R.E. Stratmann, O. Yazyev, A.J. Austin, R. Cammi, C. Pomelli, J.W. Ochterski, R.L. Martin, K. Morokuma, V.G. Zakrzewski, G.A. Voth, P. Salvador, J.J. Dannenberg, S. Dapprich, A.D. Daniels, Ö. Farkas, J.B. Foresman, J.V. Ortiz, J. Cioslowski, D.J. Fox, Gaussian, Inc., Wallingford CT (2009).

[21] M. Enamullah, M.A. Quddus, M.A. Halim, M.K. Islam, V. Vasylyeva, C. Janiak, Inorg. Chim. Acta 427 (2015) 103.

[22] C. Janiak, J. Chem. Soc., Dalton Trans. (2000) 3885–3896.

[23] (a) M. Nishio, *CrystEngComm*, 6 (2004) 130;

(b) M. Nishio, M. Hirota, Y. Umezawa, The CH/π interaction (Evidence, Nature and consequences), Wiley-VCH, 1998;

(c) Y. Umezawa, S. Tsuboyama, K. Honda, J. Uzawa, M. Nishio, Bull. Chem. Soc. Jpn. 71 (1998) 1207;

(d) C. Janiak, S. Temizdemir, S. Dechert, W. Deck, F. Girgsdies, J. Heinze, M.J. Kolm, T.G. Scharmann, O.M. Zipffel, Eur. J. Inorg. Chem. (2000) 1229–1241.

[24] M. Enamullah, G. Makhloufi, M. Refat, B.A. Joy, M.A. Islam, G. Pescitelli, D. Padula, H. Hunter, C. Janiak (submitted to *Inorg. Chem.*).

[25] M. Enamullah, M.A. Quddus, M.R. Hasan, G. Pescitelli, R. Berardozzi, G. Makhloufi, V. Vasylyeva, C. Janiak, Dalton Trans. 45 (2016) 667-680.

[26] M. Enamullah, A.K.M. Royhan Uddin, G. Pescitelli, R. Berardozzi,G. Makhloufi, V. Vasylyeva, A.-C. Chamayou, C. Janiak, Dalton Trans. 43 (2014) 3313−3329.

[27] G.S. Nichol, W. Clegg, CrystEngComm. 9 (2007) 959-960.

[28] J.W. Steed, CrystEngComm. 5 (2003) 169-179.

[29] A. Gavezotti, CrystEngComm. 10 (2008) 389-398.

[30] (a) G.R. Desiraju, CrystEngComm. 9 (2007) 91-92;

(b) J. Ruiz, V. Rodríguez, N. Cutillas, A. Hoffmann, A.-C. Chamayou, K. Kazmierczak, C. Janiak, CrystEngComm. 10 (2008) 1928-1938;

(c) V. Vasylyeva, T. Kedziorski, N. Metzler-Nolte, C. Schauerte, K. Merz, Cryst. Growth Des. 10 (2010) 4224-4226.

[31] (a) G. Althoff, J. Ruiz, V. Rodríguez, G. López, J. Pérez, C. Janiak, CrystEngComm. 8 (2006) 662-665;

(b) X. Hao, S. Parkin, C. P. Brock, Acta Crystallogr., Sect. B: Struct. Sci. 61 (2005) 689-699;

(c) N.J. Babu, A. Nangia, CrystEngComm. 9 (2007) 980-983;

(d) A.-C. Chamayou, C. Biswas, A. Ghosh, C. Janiak, Acta Cryst. C65 (2009) m311-m313;

(e) G. Makhloufi, K. Schütte, C. Janiak, Z. Kristallogr. NCS 229 (2014) 429-430;

(f) M.T. Kirchner, D. Bläser, R. Boese, G.R. Desiraju, CrystEngComm. 11 (2009) 229–231.

[32] (a) S. Roy, R. Banerjee, A. Nangia, G.J. Kruger, Chem. Eur. J. 12 (2006) 3777-3788;

(b) J.O. Hernandez, J. Portilla, J. Cobo, C. Glidewell, Acta Cryst. C71 (2015) 363–368;

(c) B.K. Sarojini, H.S. Yathirajan, E.C. Hosten, R. Betz, C. Glidewell, Acta Cryst. C71 (2015) 59–64.

[33] (a) G.S. Rodman, K.R. Mann. Inorg. Chem. 27 (1988) 3338;

(b) C. Tejel, M.A. Ciriano, M Bordonaba, J.A. Lopez, F.J. Lahoz, L.A. Oro, Inorg. Chem. 41 (2002) 2348;

(c) J.C. Bayon, G. Net, P.G. Rasmussen, J.B. Kolowich. J. Chem. Soc. Dalton Trans. (1987) 3003.

[34] (a) S.L. James, D.M.P. Mingos, X. Xu, A.J.P. White, D.J. Williams, J. Chem. Soc. Dalton Trans. (1998) 1335;

(b) R. Aumann, I.G. Schnetmann, R. Froehlich, P. Saarenketo, C. Holst, Chem. Eur. J. 7 (2001) 711;

(c) R. Bonnaire, J.M. Manoli, N. Potvin, N. Platzer, N. Goasdoue, Inorg. Chem. 20 (1981) 2691.

[35] M. Enamullah, M.A. Quddus, M.R. Hasan, G. Pescitelli, R. Berardozzi, Guido J. Reiß, C. Janiak. Eur. J. Inorg. Chem. (2015) 2758.

[36] (a) S. Yamada, Coord. Chem. Rev. 190-192 (1999) 537;

(b) T. Akitsu, Y. Einaga, Polyhedron 25 (2006) 1089;

(c) T. Akitsu, Y. Einaga. Polyhedron 24 (2005) 1869.

[37] (a) I. Veroni, A. Rontoyianni, C.A. Mitsopoulou. Dalton Trans. (2003) 255;

(b) W. Linert, M. Enamullah, V. Gutmann, R.F Jameson, Monatsh. für Chem. 125 (1994) 661;

(c) M. Enamullah, W. Linert, Thermochimica Acta 388 (2002) 401.

[38] (a) M. Enamullah, W. Linert, J. Coord. Chem. 40 (1996) 193;

(b) M. Enamullah, W. Linert, V. Gutmann, R.F Jameson, Monatsh. für Chem. 125 (1994) 1301;

(c) M. Enamullah, M.N. Uddin, D. Hossain, M. Kabir, A. Awwal, W. Linert, J. Coord. Chem. 49 (2000) 171.

[39] (a) M. Enamullah, M.K. Islam. J. Coord. Chem. 66 (2013) 4107;

(b) M. Enamullah, J. Coord. Chem. 42 (1997) 231.

[40] V. Gutmann. "The Donor-Acceptor Approach to Molecular Interactions," Plenum Press, NY, 1978.

Highlights

* Rh{(η^4-cod) or $(PPh_3)_2$}-Schiff base complexes.

* Two symmetry-independent molecules in the asymmetric unit to give a Z' = 2 structure.

* ^{31}P NMR show two doublets due to two assymetric P-atoms bound to the Rh(I) *trans* to *N* and *O* atoms, respectively.

* DFT/TDDFT calculations correspond well to the experimental results.